

High Frequency Performance of Arc Arrays Using Adaptive Beamforming

Chaoying Bao and Derek Bertilone

Defence Science and Technology Organisation, A-51, HMAS Stirling, Rockingham, WA 6958, AUSTRALIA

ABSTRACT

A baffled arc array (BAA) comprises a circular array of sensors surrounding a cylindrical metal baffle, and beamforming is carried out by processing sensors on an arc centred on beamsteer. It is widely used in sonar for passive underwater surveillance. An important factor that limits the performance of the array at high frequencies is the appearance of grating lobes in the beamformer response. This occurs when sensor separation is greater than half a wavelength, and leads to masking of weak signals by the grating lobes of strong signals. In the case of the BAA, the grating lobes are imperfect as a consequence of the circular geometry; there is a mismatch between array responses to signals arriving from the beamsteer and grating lobe directions. Adaptive beamforming is sensitive to this mismatch, and suppress the grating lobes, thus extending the frequency range of the BAA beyond its design frequency. The purpose of this paper is to demonstrate the effectiveness of adaptive beamforming for suppressing grating lobe effects in the BAA.

INTRODUCTION

Beamforming of sensor array data is used in radar, sonar and communications (Van Trees 2002). In passive sonar (Barger 1997) it is used to increase signal-to-noise ratio (SNR) of underwater acoustic signals and to indicate signal bearings. As a consequence of the discrete sampling of the wavefield by the array, grating lobes appear in the beamformer response when sensor separation is greater than half a wavelength. In the case of a uniform linear array (Van Trees 2002), the array response is identical for signals arriving from beamsteer and grating lobe directions. For a curved array, however, the array responses are distinguishable. Grating lobes still appear in the beamformer response, but are imperfect in the sense that they are not at the same level and shape as the main-lobe. An example of a curved array that is widely used in sonar is the baffled arc array (BAA). This is used to provide 360° coverage of bearings in passive underwater surveillance. It is similar to a uniform circular array (Van Trees 2002, Davis 1983) except that the sensors surround a cylindrical metal baffle, and only sensors on an arc centred on beamsteer are processed. The primary purpose of this paper is to demonstrate the effectiveness of adaptive beamformers at suppressing grating lobe effects in BAAs. Grating lobe suppression is a consequence of the sensitivity of the algorithms to mismatch between the array responses to signals arriving from the beamsteer and grating lobe directions, and is closely related to sidelobe suppression. It improves the detection of weak signals masked by strong interferers, and leads to more effective array operation when sensor separation on the arc is greater than half a wavelength.

BAFFLED ARC ARRAY (BAA)

Let Q sensors be equi-spaced around a cylindrical metal baffle. In sonar, the sensors are often physically offset (displaced) from the baffle surface, to isolate them from baffle vibrations and improve sensor coupling to the water. Acoustic signals are assumed to arrive with zero-elevation; i.e. perpendicular to the cylinder axis. In practice, each sensor (or stave) is a linear array of omnidirectional hydrophones, aligned with the cylinder axis and having phone outputs summed with zero time-delay. Thus at each stave, the phone

outputs add coherently for the signal, while ambient noise from non-zero elevations is suppressed. Only $M < Q$ staves on a cylindrical arc centred on beamsteer are processed. As the array is steered to provide 360° coverage of azimuths at zero-elevation, the arc swings around with it and selects new staves for processing. Figure 1 schematically shows the m^{th} stave and the coordinate system for the processing.

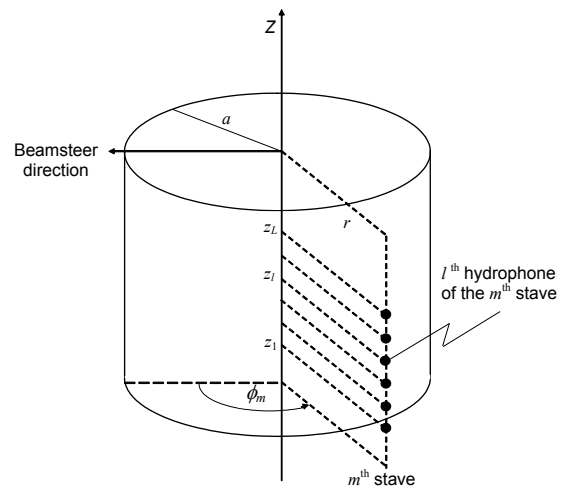


Figure 1 Coordinate system for the baffled arc array.

SENSOR RESPONSE MODEL

Referring to Figure 1, let the M sensors on the processing arc have azimuths $\phi_m, m = 1 \dots M$, assumed for convenience to be defined relative to beamsteer. At high frequencies, it is reasonable to approximate baffle scatter using infinite, rigid cylinder scattering theory (Skelton and James 1997). Suppose a plane-wave arrives with zero-elevation from beamsteer in the absence of noise. The complex narrowband output of sensor m at frequency f will be proportional to

$$\psi_m(f) = \exp(-jkr \cos \phi_m) + \sum_{n=0}^{\infty} \epsilon_n (-j)^n b_n H_n^{(1)}(kr) \cos(n \phi_m) \quad (1)$$

where

$$b_n = -\frac{J_n'(ka)}{H_n^{(1)'}(ka)} \quad (2)$$

Here r and a are the sensor radius and baffle radius respectively, $k = 2\pi f/c$ (c is sound speed in water), $H_n^{(1)}$ is the Hankel function of the first kind of order n , and ε_n is the Neumann symbol; $\varepsilon_n = 1$ for $n = 0$ and $\varepsilon_n = 2$ otherwise. Also b_n is the scattering coefficient, J_n is the Bessel function of the first kind of order n , and primes denote derivatives.

The sensor response model formulated in (1) and (2) is used for the beamforming of the BAA.

FREQUENCY-DOMAIN BEAMFORMING

To simplify notation, the beamsteer direction will be viewed as fixed so that the beamsteer variable can be dropped from all equations. Let $x_m(f)$ denote the complex narrowband output of the m^{th} sensor on the processing arc when signal and noise are present, and let $\mathbf{R}(f)$ denote the $M \times M$ cross-spectral matrix. Here $\mathbf{R}(f)$ has elements

$$r_{m,m'}(f) = \langle x_m(f) x_{m'}^*(f) \rangle \quad (3)$$

and $\langle \rangle$ is statistical expectation. A frequency-domain beamformer has mean output power

$$P(f) = \mathbf{v}(f)^H \mathbf{R}(f) \mathbf{v}(f) \quad (4)$$

where $\mathbf{v}(f)$ denotes the $M \times 1$ beamformer weight vector, and H denotes conjugate transpose.

If there are no signal distortion effects associated with baffle scatter, then conventional beamforming (CBF) can be used. In this case the elements of weight vector $\mathbf{v}(f)$ are

$$v_m(f) = a_m \frac{1}{M} \exp(-jkr \cos \phi_m) \quad (5)$$

where the a_m are array shading coefficients. However, if the sensors are offset from the baffle, then baffle scatter may distort the signal. Some compensation can be achieved by using a matched filter beamformer. In this case the weight vector is matched to a spatial replica of the signal, $\boldsymbol{\psi}(f) = [\psi_1(f) \psi_2(f) \dots \psi_M(f)]^T$ (where T denotes transpose), so that

$$\mathbf{v}(f) = \frac{\boldsymbol{\psi}(f)}{\boldsymbol{\psi}^H(f) \boldsymbol{\psi}(f)} \quad (6)$$

Finally, the Minimum Variance Distortionless Response (MVDR) beamformer is an optimum beamformer that minimises output power while fixing the response to a signal from beamsteer. In this case the weight vector is given as follows,

$$\mathbf{v}(f) = \frac{\mathbf{R}^{-1}(f) \boldsymbol{\psi}(f)}{\boldsymbol{\psi}^H(f) \mathbf{R}^{-1}(f) \boldsymbol{\psi}(f)} \quad (7)$$

Although widely referred to as MVDR in sonar, the above is also called the Minimum Power Distortionless Response (MPDR) beamformer in (Van Trees 2002), the minimum variance or maximum likelihood method in (Burdic 1991), and the Capon beamformer elsewhere.

Note that grating lobes appear in the beamformer response when $f > f_o$, where f_o is the frequency at which the sensor spacing on the arc corresponds to half a wavelength,

$$f_o = \frac{cQ}{4\pi r} \quad (8)$$

In fact, due to the geometry of the BAA, grating lobes actually appear at a frequency a little above f_o .

GRATING LOBE SUPPRESSION

The MVDR beamformer is often implemented in practice by replacing the cross-spectral matrix $\mathbf{R}(f)$ with the sample estimate computed from snapshots of data collected at different times,

$$\hat{\mathbf{r}}_{m,m'}(f) = \frac{1}{T} \sum_{t=1}^T x_m^{(t)}(f) x_{m'}^{(t)*}(f) \quad (9)$$

Here $x_m^{(t)}(f)$, $t = 1 \dots T$ are narrowband outputs of sensor m collected at times indexed by t . When this estimate is recomputed for each block of received data, MVDR becomes an adaptive algorithm known as MVDR with sample matrix inverse, or MVDR SMI.

Figure 2 shows FRAZ (FREquency-AZimuth) spectra computed from actual sea trials data. A BAA with $Q = 32$ sensors in total and $M = 8$ sensors on the processing arc was used, two seconds of data was processed, and $T = 62 \times M$ snapshots utilised. Noise spectral equalisation was applied to each FRAZ. The FRAZ at top shows CBF with modified offset raised cosine (MORC) shading. This shading is obtained by projecting the widely used offset raised cosine shading for linear arrays onto the curved geometry. A strong signal is at bearing 180° . The grating lobes are the strong structures that are at either side of the signal and appear at the frequencies above approximately $1.1f_o$. They are quite severe and can be distinguished from the main-beam sidelobes that have lower power and thinner beams. The middle FRAZ shows MVDR SMI and demonstrates the significant reduction in grating lobe effects that is achievable in practice.

Adaptive beamformers are required to be robust for practical implementation (Van Trees 2002). The bottom image in Figure 2 shows a FRAZ computed using a robust adaptive algorithm proposed by Li, Stoica and Wang (Li etc 2003). This is a robust version of MVDR that improves the signal response when knowledge of the steering vector is imprecise (due to pointing errors or baffle model errors, for example). The algorithm anticipates possible errors in the signal model. The actual signal response vector, $\boldsymbol{\psi}_a$, is estimated by solving the following quadratic problem,

$$\min_{\boldsymbol{\psi}_a} \boldsymbol{\psi}_a^H \hat{\mathbf{R}}^{-1} \boldsymbol{\psi}_a \quad \text{subject to } \|\boldsymbol{\psi}_a - \boldsymbol{\psi}\|^2 \leq \varepsilon, \quad (10)$$

where ε is a small positive number proportional to the signal mismatch, and is called the steering vector error bound. Once $\boldsymbol{\psi}_a$ is obtained (see (Li etc 2003) for details), the solution for \mathbf{v} can be computed using the formula:

$$\mathbf{v} = \frac{\hat{\mathbf{R}}^{-1} \boldsymbol{\psi}_a}{\boldsymbol{\psi}_a^H \hat{\mathbf{R}}^{-1} \boldsymbol{\psi}_a} \quad (11)$$

Although essentially a diagonal loading approach, better results are obtained than by direct loading of the sample cross-spectral matrix. The steering vector error bounds are required as an input to the algorithm, and in the case of Figure 2, the error bounds were chosen so as to roughly optimise signal bearing resolution. Grating lobe suppression is excellent, and was maintained when error bounds were increased to accommodate a sensor failure.

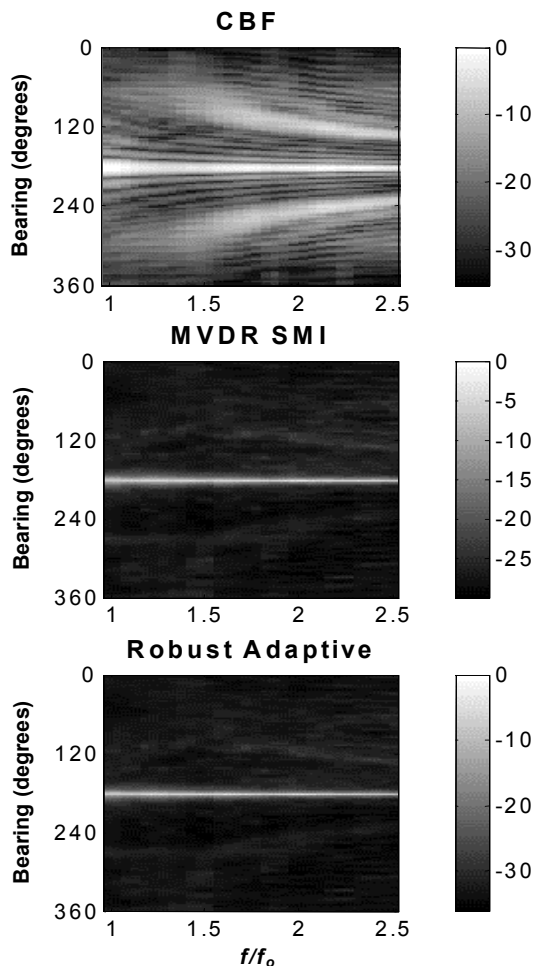


Figure 2 FRAZ (Frequency-Azimuth) plots for sea trials data with a contact at 180°.

PASSIVE SONAR APPLICATION

Sonar operation is dramatically improved by the suppression of grating lobes. Figure 3 shows bearing-time (BT) plots of real sonar data with a group of strong contacts just at left of centre. CBF with MORC shading is shown at top, and robust adaptive beamforming at bottom. Each scan was obtained by computing a FRAZ and summing frequency bins in the band f_0 to $2.5f_0$. Time and bearing are denoted by index, and the full range of bearings is not shown. Display processing was identical in both cases, and included histogram modification to enhance the visibility of weak signals (the 30% lowest power pixels were set to the same level, and similarly the 3% highest power pixels). Although the main-beam sidelobes are not evident due to the smoothing effect of the frequency integration, CBF exhibits a prominent grating lobe band on either side of the group of strong contacts. This masks the presence of a weak contact that initially lies to the right of the strong contacts and rapidly changes bearing after time index 100. Adaptive beamforming suppresses the grating lobes to clearly reveal the weak contact. It also reveals a group of weak contacts just to the left of the strong contacts.

CONCLUSION

Adaptive beamforming is effective at suppressing grating lobe effects in curved arrays, thereby enhancing detection of weak signals masked by strong interferers, and significantly improving array operation when sensor separation is greater than half a wavelength. The effectiveness of the suppression was demonstrated for a BAA by applying adaptive beamformers to real sonar data. If the sensors are offset from the baffle surface, then the acoustic wavefield sampled by the sensors is spatially distorted at high frequencies due to interference between incident and scattered fields. For a conventional beamformer, the grating lobe/sidelobe structures are severely distorted, and can have power exceeding that of the signal. In this situation the conventional beamformer essentially fails. By comparison, the MVDR beamformer continues to give an appropriate angular response.

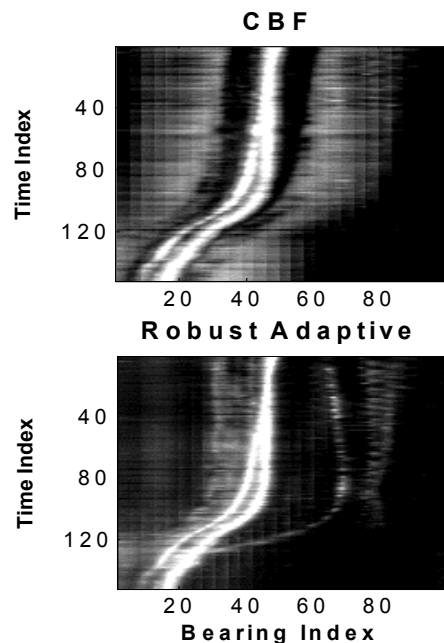


Figure 3 Bearing-time plots for sea trials data with multiple contacts.

REFERENCES

Barger, J. E. (1997) *Sonar systems. in Encyclopedia of acoustics. Vol.1*, Crocker, M. J., Ed. Wiley.
 Burdic, W. S. (1991) *Underwater acoustic system analysis*. Prentice Hall.
 Davies, D. E. N. (1983) *Circular arrays. in The handbook of antenna design, Vol.2*, Rudge, A. W., Milne, K., Olver, A. D. and Knight, P., Eds. Peter Peregrinus.
 Skelton, E. A., and James, J. H. (1997) *Theoretical acoustics of underwater structures*. Imperial College Press.
 Li, J., Stoica, P., and Wang, Z. (2003) *On robust capon beamforming and diagonal loading*, IEEE Trans. Signal Processing, Vol.51 (7), pp.1702-1715.
 Van Trees, H. L. (2002) *Optimum array processing, part IV of detection, estimation and modulation theory*. Wiley-Interscience.